Measuring angular diameters of extended sources

P.A.M. van Hoof[★]

Kapteyn Astronomical Institute, P.O. Box 800, 9700 AV Groningen, The Netherlands
University of Kentucky, Department of Physics and Astronomy, 177 CP Building, Lexington, KY 40506–0055, USA

arXiv:astro-ph/9912239v1 10 Dec 1999

ABSTRACT

When measuring diameters of partially resolved sources like planetary nebulae, H II regions or galaxies, often a technique called gaussian deconvolution is used. This technique yields a gaussian diameter which subsequently has to be multiplied with a conversion factor to obtain the true angular diameter of the source. This conversion factor is a function of the FWHM of the beam or point spread function and also depends on the intrinsic surface brightness distribution of the source.

In this paper conversion factors are presented for a number of simple geometries: a circular constant surface brightness disk and a spherical constant emissivity shell, using a range of values for the inner radius. Also more realistic geometries are studied, based on a spherically symmetric photo-ionization model of a planetary nebula. This enables a study of optical depth effects, a comparison between images in various emission lines and the use of power law density distributions. It is found that the conversion factor depends quite critically on the intrinsic surface brightness distribution, which is usually unknown. The uncertainty is particularly large if extended regions of low surface brightness are present in the nebula. In such cases the use of gaussian or second moment deconvolution is not recommended.

As an alternative, a new algorithm is presented which allows the determination of the intrinsic FWHM of the source using only the observed surface brightness distribution and the FWHM of the beam. Hence no assumptions concerning the intrinsic surface brightness distribution are needed. Tests show that this implicit deconvolution method works well in realistic conditions, even when the signal-to-noise is low, provided that the beam size is less than roughly 2/3 of the observed FWHM and the beam profile can be approximated by a gaussian. A code implementing this algorithm is available.

Key words: Methods: data analysis — ISM: general

1 INTRODUCTION

The accurate measurement of angular diameters is a long standing problem. It is pertinent to the study of planetary nebulae, H II regions, galaxies and other extended sources. Nevertheless, only few papers dedicated to this problem can be found in the literature, e.g. Mezger & Henderson (1967), Panagia & Walmsley (1978), Bedding & Zijlstra (1994), Schneider & Buckley (1996), and Wellman et al. (1997). This paper will be written in the context of planetary nebula research. However, most results will also be valid in a more general context.

Several methods are in general use to determine angular diameters. For nebulae with a well-defined outer radius (i.e. with a steep drop-off to zero surface brightness at a certain radius) it is easy to measure directly the radius where a prescribed value of the surface brightness is reached. This prescribed value often is a certain fraction of the peak surface brightness (usually 10 %). This method will be called direct measurement. It is in general use for observations of well-resolved sources and will not be studied in this paper. This method works, provided that observations of sufficient resolution and quality are available. This way no assumptions have to be made about the intrinsic surface brightness distribution of the source and this explains the popularity of this method. It should be pointed out that in *all* other cases (i.e. when the source is not well resolved or when it does not have a well-defined outer radius) assumptions have to be made about the intrinsic surface brightness distribution in order to interpret the results. In the remainder of the paper we will also refer to the surface brightness distribution as surface brightness profile or simply profile.

For observations where the source is only partially resolved, one has to resort to different methods. One method is based on the Full Width at Half Maximum (FWHM) of a two-

---

[★] Currently staying at CITA, University of Toronto, Canada.

dimensional gaussian fitted to the observed surface brightness distribution in a least-squares sense. This method is usually called gaussian deconvolution and will be explained in more detail below. Another method that is being used is basically identical to the first, except that it determines the FWHM using the second moment of the surface brightness distribution instead of a gaussian fit. To discriminate it from the first method, it will be called second moment deconvolution. The choice for either method depends mainly on the preference of the observer. Both methods have the disadvantage that they yield a result that has no direct physical meaning. Hence, a conversion factor is needed to translate the result into something meaningful. In nebular research this usually is the Strömgren radius. This conversion factor depends on the method being used, the intrinsic surface brightness distribution of the source and the size of the beam.

Another problem is that not all nebulae have a well-defined outer radius. Often, when deeper images are made, more emission is detected at lower surface brightness levels. Such nebulae will be referred to as having a soft boundary. For such nebulae the 10 % radius (or a radius at any other percentage level) does not have a direct physical meaning and does not represent the nebular size very well. The radius becomes increasingly larger when deeper images are taken. The Strömgren radius can usually not be observed directly either. Hence the size of such nebulae cannot be represented in a meaningful way by a single number. In Section 7 it will be shown that also the application of gaussian or second moment deconvolution to such nebulae leads to large uncertainties and cannot be recommended.

The major disadvantage of gaussian and second moment deconvolution is that assumptions have to be made about the shape (but not the size) of the intrinsic surface brightness distribution of the source. It will be shown in this paper that this choice is quite critical. However, when only low resolution observations are available one can make no more than an educated guess about this distribution. As an alternative, a new algorithm is presented which allows the determination of the intrinsic FWHM of the source using only the observed surface brightness distribution and the FWHM of the beam. Hence the major advantage of this method is that it yields a deconvolved diameter without necessitating assumptions concerning the intrinsic surface brightness distribution. This process is *not* an image reconstruction algorithm and therefore requires far less computational overhead. It should be pointed out that it can only give the FWHM diameter and not the Strömgren diameter. For the latter conversion, assumptions concerning the shape of the nebula will always be necessary.

This article will have the following structure: in Section 2 some basic assumptions and definitions will be given. Also, the methods used to calculate the conversion factors will be discussed. In Section 3 conversion factors will be given for various simple geometries: a circular constant surface brightness disk and a spherical constant emissivity shell, using a range of values for the inner radius. In Section 4 these results will be compared to previous studies found in the literature and a discussion will be given. Next, the conversion factors will be studied using more realistic geometries based on a photo-ionization model of a planetary nebula. In Section 5 the influence of optical depth effects on the observed surface brightness distribution and on the conversion factor will be studied. In Section 6 images constructed in several optical emission lines will be compared and the influence on the conversion factor will be discussed. In Section 7 the effect of non-constant density laws on the conversion factor will be studied. These density laws allow a discussion of the appropriateness of gaussian or second moment deconvolution for nebulae with a soft boundary. In Section 8 a new method will be presented which allows the determination of the intrinsic FWHM of a profile, using only the observed profile and the beam size. Finally, in Section 9 the main conclusions will be presented. The theory used to calculate the conversion factors has been presented in van Hoof (1998) (hereafter Paper I). This paper is available through the e-print archive at `http://xxx.lanl.gov` under number astro-ph/9906051.

2 DEFINITIONS AND COMPUTATIONAL METHODS

The methods discussed in this article can be applied to observations at any wavelength. More in particular, they are valid for optical, infrared and radio observations. The resolution of these observations is usually characterized by the size of the beam profile for radio data and by the size of the point spread function for optical or infrared data. Throughout the paper the term 'beam' will be used and it will be implicitly understood that it can also mean 'point spread function' where appropriate. It will be assumed that the beam can be approximated by a gaussian. This is a reasonable assumption, both for radio and for optical observations. First, in the reduction of radio observations, the (possibly complicated) antenna pattern of the telescope is replaced by a perfect gaussian of the same resolution in the CLEAN procedure. Second, for optical observations the point spread function is normally determined by the seeing which can be approximated by a gaussian. This approximation is however only valid for the core region of the point spread function, further out it is better represented by an inverse square law (e.g., King 1971). This implies that care should be taken when interpreting low level emissions surrounding barely resolved nebulae; accurate knowledge of the point spread function is required in such cases (Falomo 1996). In this paper the intrinsic surface brightness profile will be defined as the surface brightness distribution that would be observed with infinite resolving power. For simplicity it will be assumed throughout this paper that both the surface brightness distribution of the nebula and the beam are circularly symmetric. This is a rather severe restriction; nebulae rarely are circular and also, for radio observations, the beam usually is elliptical. However, this simplified case already yields interesting results which can be applied to actual data. Since both the intrinsic profile of the nebula and the beam profile are assumed to be circularly symmetric, they can be represented as one-dimensional functions measuring the profile radially outwards from the centre.

As was already remarked, a conversion factor is needed to translate the FWHM diameter yielded by gaussian or second moment deconvolution into a Strömgren diameter. In this paper the Strömgren radius of the nebula will be denoted by r_s, and the true diameter by $\Theta_d = 2r_s$. The FWHM of the observed nebular image will be denoted by Φ and the

FWHM of the beam by Φ_{b}. Throughout the paper the deconvolved FWHM diameter Φ_{d} will be used, which is defined by

$$\Phi_{\mathrm{d}} = \sqrt{\Phi^2 - \Phi_{\mathrm{b}}^2}. \tag{1}$$

This quantity is also commonly called the gaussian diameter. The conversion factor to obtain the true angular diameter from the deconvolved FWHM can be defined as

$$\Theta_{\mathrm{d}} = \gamma\Phi_{\mathrm{d}} \quad \Rightarrow \quad \gamma = \Theta_{\mathrm{d}}/\Phi_{\mathrm{d}} = 2r_{\mathrm{s}}/\Phi_{\mathrm{d}}. \tag{2}$$

The deconvolved FWHM should *not* be confused with the FWHM of the deconvolved profile, which in general will not be equal. The latter will be called the intrinsic FWHM. The conversion factor γ is a function of the resolution of the observation, or to be more precise, of the ratio of the source diameter and the beam size. Hence an independent parameter β is chosen, which is defined as

$$\beta = \Phi_{\mathrm{d}}/\Phi_{\mathrm{b}}. \tag{3}$$

In the following sections more details will be given of the techniques that have been used to calculate the conversion factors, both for gaussian and second moment deconvolution.

2.1 Gaussian deconvolution

First the technique that has been used to calculate conversion factors for gaussian deconvolution will be discussed. This technique is based on an implicit equation from which the value of $\gamma(\beta)$ can be solved for arbitrary β. The derivation of this expression has been presented in Section 3 of Paper I. To use this technique, first the radial moments c_n of the assumed intrinsic surface brightness profile $f(r)$ have to be computed. They are defined as:

$$c_n = 2\pi \int_0^\infty f(r) r^{n+1} \mathrm{d}r,$$

and are computed using either an analytic expression (if available) or a numerical integration scheme. Next these radial moments and also the value for β are substituted in Eq. (4).

$$\sum_{n=0}^\infty \frac{c_{2n}\gamma^{2n}(\beta)\ln^n 2}{n!} \sum_{k=0}^n (-1)^{n-k} \binom{n}{k} \times$$
$$\times (\beta^2 - 2k)\,\beta^{2n-2} \left(\frac{\beta^2+1}{\beta^2+2}\right)^k = 0. \tag{4}$$

The value for the conversion factor γ is solved iteratively using a Newton-Raphson scheme. If this procedure is repeated for a range of values for β, the behaviour of the conversion factor $\gamma(\beta)$ as a function of β can be found.

In order to represent the results efficiently, a simple analytic function will be fitted to the conversion factors. Tests have shown that $\gamma(\beta)$ can be approximated extremely well by the following function

$$\gamma_f(\beta) = \frac{a_1}{1 + a_2\beta^2} + a_3, \tag{5}$$

which will be used throughout this paper. The fit is determined by minimizing the reduced χ^2 which is defined as

$$\chi^2 = \frac{1}{N} \sum_{n=1}^N \left[\gamma(\beta_n) - \gamma_f(\beta_n)\right]^2. \tag{6}$$

Here N is the total number of points at which the conversion factor has been evaluated (usually 251, with $\beta_n = 0\,(0.02)\,5)^{\dagger}$.

2.2 Second moment deconvolution

Second moments are widely used to calculate the FWHM of an arbitrary profile. In general however, the result of this method will not be identical to the FWHM derived from a gaussian fit. Hence, also the value for the conversion factor will be different. To distinguish the results of the two methods, a subscript 2 will be used on all quantities derived with the second moments method. In Paper I, Section 5 it has been proven that when second moment deconvolution is used, the conversion factor is constant (i.e. *independent* of beam size). Furthermore, this constant value is equal to the value of the conversion factor for gaussian deconvolution in the limit for infinitely large beams. In other words, the conversion factor for second moment deconvolution is given by

$$\gamma_2(\beta) = \gamma(0) \quad \text{for all } \beta \in [\,0, \infty). $$

Due to this relation it is not strictly necessary to give separate results. The value for the conversion factor for second moment deconvolution can always be calculated using the following expression

$$\gamma_2 \approx \gamma_f(0) = a_1 + a_3. \tag{7}$$

Given the quality of the fitting function γ_f, this yields results with more than sufficient accuracy (a few times 10^{-3} down to a few times 10^{-4}).

3 THE CONVERSION FACTOR FOR SIMPLE GEOMETRIES

The methods which have been discussed in the previous section are applied to images which are only partly resolved. Hence they contain little direct information on the intrinsic surface brightness profile. If no other information is available, the intrinsic surface brightness profile has to be assumed in order to calculate the conversion factor. In such cases, the choice is usually a very simple geometry. In this section, conversion factors will be determined for the geometries that where presented in Bedding & Zijlstra (1994). These are the constant surface brightness disk (the limiting case of a spherically symmetric nebula which is completely optically thick, or alternatively a nebula with cylindrical symmetry viewed along the axis), and the constant volume emissivity shell and sphere (the limiting case of a spherically symmetric nebula with zero optical thickness). These cases will be treated in more detail here, and also shells with an arbitrary inner radius will be treated. The sphere can be viewed as the limiting case of a shell with zero inner radius.

---

† This notation indicates that β_n runs from 0 to 5 with a step size of 0.02.

Table 1. The parameters for calculating conversion factors. Results are given for a constant surface brightness disk and for a constant emissivity shell with various ratios of the inner to outer radius (as indicated in column 1). The conversion factors for gaussian deconvolution can be calculated using Eq. (5), the conversion factors for second moment deconvolution are given separately in the last column.

case	a_1	a_2	a_3	χ^2	γ_2
disk	0.3512	0.7874	1.3469	$5.4(-8)^\dagger$	1.6986
shell 0.0	0.3358	0.7907	1.5629	4.1(−8)	1.8991
shell 0.1	0.3368	0.7896	1.5609	4.3(−8)	1.8982
shell 0.2	0.3431	0.7835	1.5482	5.1(−8)	1.8918
shell 0.3	0.3563	0.7745	1.5187	6.3(−8)	1.8756
shell 0.4	0.3729	0.7694	1.4733	6.8(−8)	1.8468
shell 0.5	0.3875	0.7715	1.4168	6.5(−8)	1.8049
shell 0.6	0.3959	0.7786	1.3546	6.1(−8)	1.7510
shell 0.7	0.3963	0.7871	1.2909	5.9(−8)	1.6877
shell 0.8	0.3893	0.7940	1.2281	5.7(−8)	1.6180
shell 0.9	0.3766	0.7981	1.1678	5.4(−8)	1.5449
limit 1.0	0.3600	0.7994	1.1106	5.0(−8)	1.4711

$\dagger$ $5.4(-8)$ stands for 5.4×10^{-8}.

**Table 2.** The conversion factor and the FWHM for the unconvolved disk and shell profiles.

case	$\gamma(\infty)$	$\Phi/r_{\rm s}$
disk	1.346 346	1.485 502
shell 0.0	1.562 397	1.280 084
shell 0.1	1.560 415	1.281 710
shell 0.2	1.547 616	1.292 310
shell 0.3	1.518 086	1.317 449
shell 0.4	1.472 623	1.358 121
shell 0.5	1.416 124	1.412 306
shell 0.6	1.353 972	1.477 135
shell 0.7	1.290 243	1.550 095
shell 0.8	1.227 504	1.629 323
shell 0.9	1.167 188	1.713 520
limit 1.0	1.110 004	1.801 795

### 3.1   The constant surface brightness disk

The conversion factors for gaussian deconvolution are shown in Fig. 1 and the parameters for the fit are given in Table 1. The residuals of the fit are also shown in Fig. 1. Additionally, the conversion factor for second moment deconvolution is given in Table 1. In Table 2 the conversion factor and the FWHM for the unconvolved profile are given. These numbers are intended as benchmarks and can be useful for testing gaussian fit algorithms. The values were calculated using Eq. (8), which can be solved using a Newton-Raphson scheme.

$$\sum_{n=0}^{\infty}(-1)^n\,(2n+1)\,\frac{c_{2n}\,\gamma^{2n}\,\ln^n 2}{n!} = 0; \quad \frac{\Phi}{r_{\rm s}} = \frac{2}{\gamma}. \qquad (8)$$

This formula can derived from Eq. (4) by taking the limit $\beta \to \infty$. It constitutes a new way of measuring the FWHM of an observed profile and is discussed in more detail in Paper I. The values given in Table 2 are accurate in all decimal places.
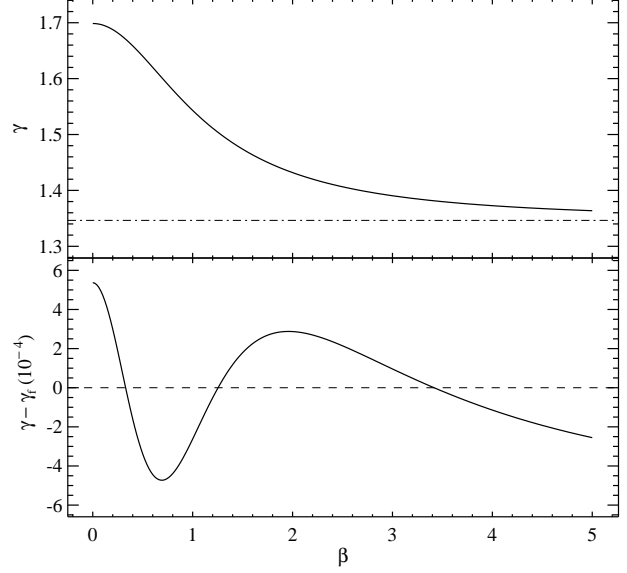
Figure 1. The conversion factors for a constant surface brightness disk (upper panel) and the residuals of the fit to these conversion factors (lower panel). The dash-dotted line in the upper panel indicates the value for $\gamma(\infty)$.
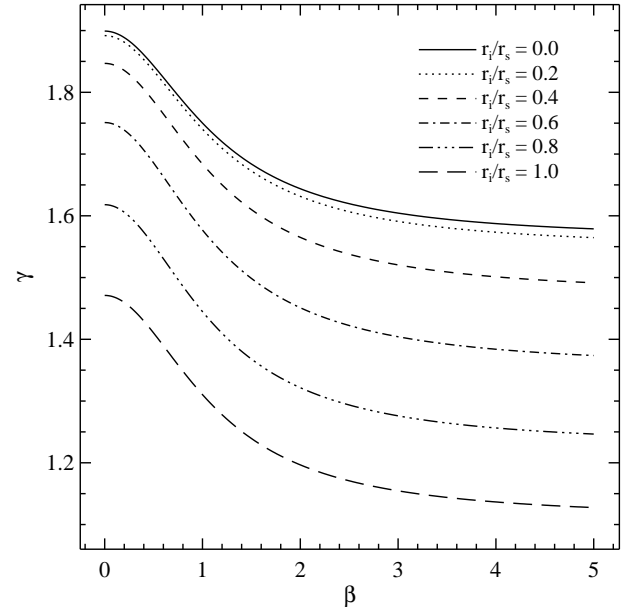
Figure 2. The conversion factor for constant emissivity shells, for various ratios of the inner to outer radius ($r_{\rm i}/r_{\rm s}$).

3.2   The constant emissivity shell

Conversion factors were also computed for the case of a constant emissivity shell with a range of values for the ratio of the inner to outer radius: $r_{\rm i}/r_{\rm s} = 0.0$ (0.1) 1.0. The results are shown in Fig. 2 and the fit parameters are given in Table 1. Again the quality of the fits is very good. It can be seen that the shape of the curve doesn't change very much as a function $r_{\rm i}/r_{\rm s}$, but that the height of the curve does. This means that the correct value for the conversion factor does

depend quite critically on the assumed value for the inner radius. The conversion factors for second moment deconvolution are also given in Table 1. The conversion factor and the FWHM for the unconvolved profiles are given in Table 2. See also the remarks in Section 3.1.

4   COMPARISON OF THE RESULTS

In this section the results from Section 3 will be compared with other results. First, the conversion factors will be compared to the results from a more straightforward approach. This is done to verify the correctness of the procedure used in this paper. This comparison will be limited to the geometries that were already studied in the literature: the constant surface brightness disk, the constant emissivity sphere and the constant emissivity shell with $r_i/r_s = 0.8$. Next, the results from this paper will be compared to published data.

4.1   Comparison with a different technique

In order to verify the procedure described in Section 2.1 for calculating conversion factors for gaussian deconvolution, a more straightforward approach was used to check the results. This technique essentially mimics the procedure used in real observations: a given intrinsic surface brightness profile is convolved with a gaussian of prescribed width and subsequently gaussian deconvolution is applied using a standard gaussian fit routine. In order to distinguish the two techniques, the procedure described in Section 2.1 will be called method A, and the procedure described here will be called method B. The reason that method A was adopted throughout the paper is that it is by far the fastest and most accurate method.

For the three geometries that have been mentioned above, the results of method A were found to be in excellent agreement with the results of method B. For the disk case it was found that $\chi^2 = 4.6 \times 10^{-7}$, for the shell case $\chi^2 = 7.4 \times 10^{-8}$ and for the sphere case $\chi^2 = 3.0 \times 10^{-8}$ (see Eq. 6). This proves the correctness of method A. The comparison is also visualized in Fig. 3.

Since the calculation of the conversion factors for second moment deconvolution is closely linked to the calculation of the conversion factors for gaussian deconvolution (see Section 2.2), this also proves the correctness of our results for the second moment method.

4.2   Comparison with published results

Four papers have been previously published which were (at least in part) dedicated to calculating conversion factors for circularly symmetric profiles. These are Mezger & Henderson (1967) (hereafter MH), Panagia & Walmsley (1978) (hereafter PW), Bedding & Zijlstra (1994) (hereafter BZ) and Schneider & Buckley (1996) (hereafter SB). A comparison of all the results is shown in Fig. 3. It should be noted that in all these papers the gaussian deconvolution method was used. Second moment deconvolution has never been studied before in the literature and hence no comparison can be given for the results of this method.

Mezger & Henderson (1967) assumed that conversion factors are independent of the beam size. They derived the
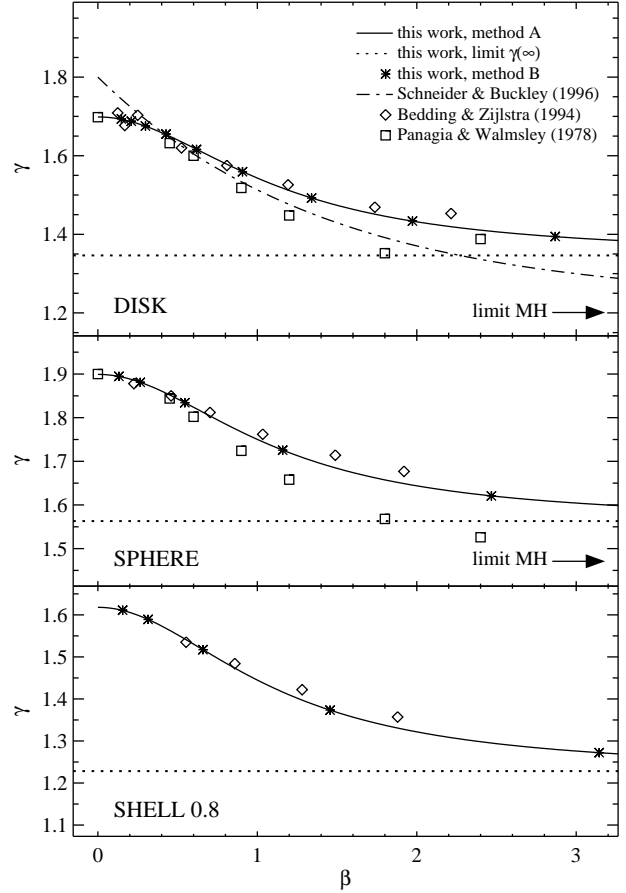

Figure 3. Comparison of this work with previous results. Methods A and B are explained in the text. The arrows 'limit MH' indicate the value for $\gamma(\infty)$ obtained by Mezger & Henderson (1967).

conversion factors by comparing the diameter of an unconvolved disk or sphere to a gaussian with the same peak surface brightness and total flux. Hence one could say that they assumed $\beta = \infty$. However their method is clearly not appropriate, since fitting a gaussian to a given profile does not conserve the flux nor does it conserve the peak surface brightness. It can be seen that their results are substantially lower than the results from this study.

Panagia & Walmsley (1978) re-examined the conversion factors for both geometries. They concluded that the conversion factors depend on the beam size and that adopting the results of MH will generally lead to an underestimation of the nebular diameter. The value of the conversion factor for $\beta = 0$ was calculated using an analytic expression. The method they used to calculate the other points is not clearly described. It can be seen that for $\beta = 0$ their results coincide with the results of this paper. However, for larger β an increasing discrepancy between the results becomes apparent. In the disk case they even find a minimum in $\gamma(\beta)$ which is not reproduced in this work. These discrepancies will be discussed together with the results of SB.

Bedding & Zijlstra (1994) re-examined the conversion factors for the disk and the sphere case and also added the case of a shell geometry. The method they used was essen-
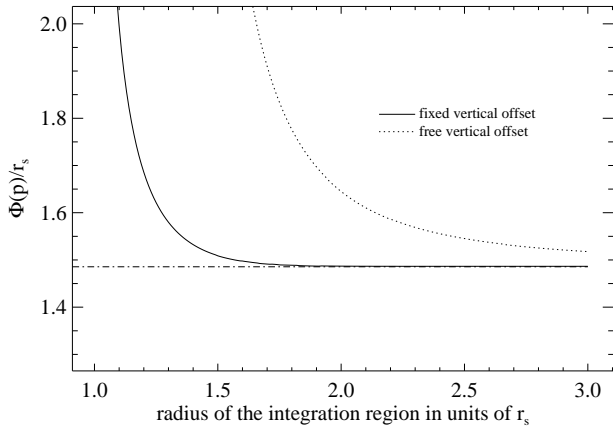
Figure 4. The FWHM resulting from a gaussian fit to a constant surface brightness disk as a function of the radius of the fitting region. The dash-dotted line indicates the value of the FWHM for an infinitely large fitting region, i.e. the correct value given in Table 2.

tially identical to method B. Dr. Zijlstra kindly provided me with a table from which the values of β and γ could be determined. These results are clearly the most accurate of all literature data. It seems BZ systematically make a slight overestimation of the conversion factor for larger values of β. An explanation for this is not apparent to the author.

Schneider & Buckley (1996) studied only the disk geometry. They were the first to use an analytic fit to the conversion factor as a function of β. The method they used was essentially identical to method B. In their results it can be seen that the conversion factor is progressively underestimated for larger β. The most likely explanation for this result (and also for the results of PW) is as follows. The gaussian fit to the (convolved) surface brightness profile is determined by minimizing the quadratic residuals, which is defined as an integral over an infinite region. In a numerical code this integral is replaced by an integral over a finite region, where the upper limit of this region should be large enough not to influence the result. If the upper limit is chosen too low, the fit will not be 'punished' for the tails of the gaussian outside the integration region. In the case of a disk geometry this will lead to an overestimation of the FWHM as is shown in Fig. 4 (solid curve). In view of this result, it is recommended to use a diameter for the fitting region which is at least 3 times the FWHM diameter of the fit, irrespective of the fact if the nebula has a non-zero surface brightness in the whole of this region or not. For nebulae with extended faint emission the integration region should encompass the whole of the nebula of course. In the case where the surface brightness profile is a perfect gaussian (which is the case in the limit for infinitely large beam sizes, $\beta = 0$), the mentioned effect does not exist. The residuals will be zero everywhere and the upper limit of the integration region is irrelevant. The bigger the discrepancy between the actual profile and a perfect gaussian is (i.e. the larger β is), the stronger the fit will be affected by the effect. This is exactly what can be seen in the results of PW and SB. The local minimum that was found by PW for the disk case may have been caused by the fact that they used a larger integration

region for the last point, although this is not clear from their paper.

Another point of caution is the following. In order to obtain an accurate value for the FWHM of an observed source, it is essential that the global background in the image is subtracted first so that it can assumed to be zero in the fitting procedure. This was done to produce the solid curve in Fig. 4. One might be tempted to try and determine the FWHM and the background simultaneously in the fitting procedure. However, this gives very bad results as is indicated by the dotted curve in Fig. 4. Here a gaussian $a_1 \exp(-a_2 r^2) + a_3$ was fitted to the constant surface brightness disk, treating a_3 as a free parameter. One can readily see that the results are poor. The radius of the fitting region has to be very large to get even moderately accurate results. The cause of this is that the fit is not punished for the fact that the gaussian drops below the background at infinity, which in turn gives it the freedom to make the gaussian wider and thus obtain a better fit inside the integration region.

For very small values of β, SB find higher values for the conversion factor than this study. This is probably an artifact of the fitting function adopted by SB. It was found to give lower quality fits than the fitting function adopted in this paper, while it has the same number of free parameters. The conversion factor $\gamma(\beta)$ has a first derivative which is zero at $\beta = 0$, as is also the case for the fitting function adopted in this paper. This is however not the case for the fitting function adopted by SB. Since it is impossible to compute the conversion factor for very small β using method B (as was done by SB), their fit will not be constrained for those values and thus their choice of fitting function will give results which are too high near $\beta = 0$.

When the results of PW are viewed for large beam sizes, it can be seen that the conversion factor is roughly 1.7 in the disk case, and roughly 1.9 in the sphere case. This had led to the popular notion that the deconvolved FWHM should be multiplied by 1.8 to obtain the correct diameter, independent of beam size and intrinsic surface brightness distribution. The popularity of this assumption should in all probability be attributed to its simplicity. However, from the previous discussion it becomes clear that quite substantial errors can be made this way, as was already pointed out by PW. The magnitude of this error can easily be greater than the observational uncertainties in the measurement itself. Hence this simplification cannot be justified. This implies that assumptions about the intrinsic surface brightness profile are unavoidable. Since there obviously is room for discussion about these assumptions, the author would like to urge all observers to publish besides the derived angular diameter (which depends on these assumptions) also both the deconvolved FWHM (which does not depend on these assumptions) *and* the beam size.

5   OPTICAL DEPTH EFFECTS

In the previous sections several simple geometries have been studied where an analytic expression for the intrinsic surface brightness profile can be assumed. However, in the following sections more realistic geometries will be studied. These will be based on a photo-ionization model of a planetary

Table 3. The parameters for calculating conversion factors in different observing modes. The conversion factors for gaussian deconvolution can be calculated using Eq. (5), the conversion factors for second moment deconvolution can be calculated using Eq. (7).

case	a_1	a_2	a_3	$\tau^\dagger$
radio 2 cm	0.3428	0.7853	1.6222	1.44(-2)
radio 6 cm	0.3429	0.7860	1.6067	1.46(-1)
radio 20 cm	0.3462	0.7892	1.4767	1.81($+0$)
radio 60 cm	0.3529	0.7870	1.3708	1.79($+1$)
radio 200 cm	0.3433	0.7854	1.3753	2.18($+2$)
Hα	0.3605	0.7822	1.4937	4.53(-1)
Hα+[N II]	0.3569	0.7867	1.3656	4.53(-1)
Hβ	0.3644	0.7817	1.4842	6.30(-1)
[O III]	0.4083	0.7892	1.3176	6.11(-1)

† The optical depth is measured from the centre of the nebula to the outer edge.

nebula. The procedure to calculate the conversion factors in this case is as follows. A table with the emissivity and the absorption coefficient as a function of distance to the star is calculated with a modified version of the photo-ionization code CLOUDY 84.12a (Ferland 1993). When the emissivities and the absorption coefficients are known, the radiative transport equation can be integrated numerically, assuming spherical symmetry and neglecting scattering processes. This is done by a separate code which yields an intrinsic surface brightness profile. This profile can then be used to determine the conversion factors using the procedure already described in Section 2.1.

To study the effect of varying optical depth with wavelength, the results of the planetary nebula model at various wavelengths in the radio regime have been used. The physical process responsible for emission and absorption at these wavelengths is free-free interaction between protons and electrons. It is a well known fact that the optical depth τ due to free-free absorption increases towards longer wavelengths as $\tau \propto \lambda^{2.1}$ (e.g., Pottasch 1984). The input parameters for CLOUDY were taken from the NGC 7027 model discussed in Beintema et al. (1996). This nebula was chosen solely for the purpose of getting a realistic model. The fact that NGC 7027 is quite large and thus well resolved in most observations is of no importance. One could assume that another nebula is modelled which is very similar to NGC 7027, but at a much larger distance. Using this model, the shape of the surface brightness profile at various wavelengths could be determined. It turns out that the surface brightness profile is very sensitive to optical depth effects. To illustrate this, various profiles are shown in the upper panel of Fig. 5. The conversion factors to obtain the true angular diameter at the various wavelengths are shown in the lower panel of Fig. 5. The nebula is only marginally optically thick at 6 cm, but this already has a noticeable effect on the conversion factor. At 20 cm the nebula is mildly optically thick, and this has a strong effect on the conversion factor.

The effect may be less in other nebulae. However, in general this cannot be assumed *a priori*, and thus care should be taken when comparing measurements taken at different wavelengths. This is not only true because of the effects described above, but also because at different wavelengths the
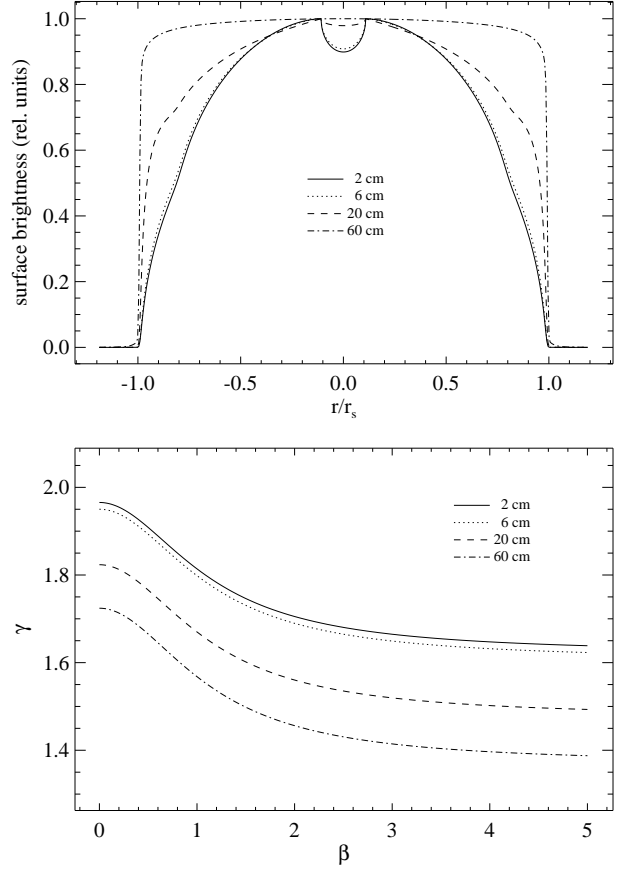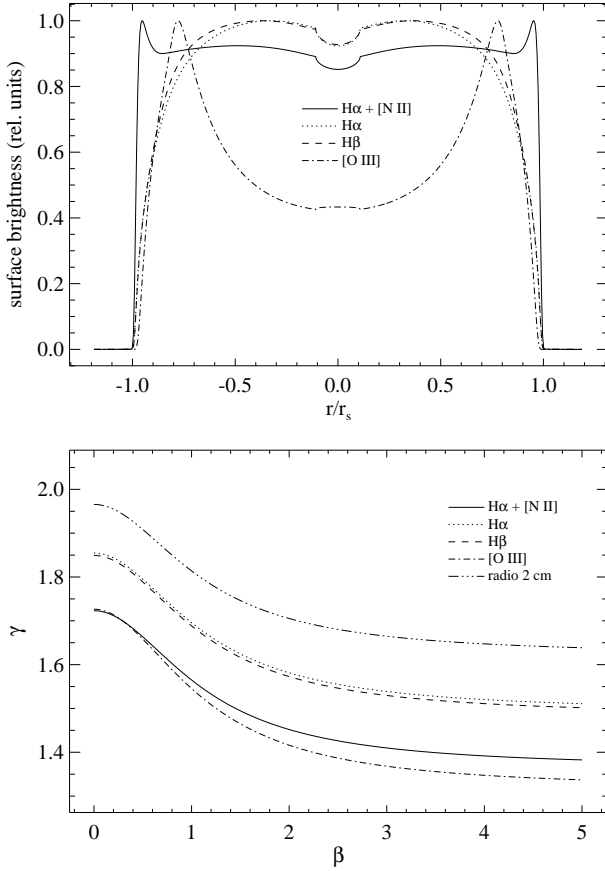

Figure 5. The surface brightness profiles (upper panel) and the conversion factors (lower panel) computed at wavelengths of 2 cm, 6 cm, 20 cm and 60 cm. The maximum surface brightness has been normalized to unity.

beam size will be different, hence β will be different and this will influence the conversion factor as well when gaussian deconvolution is used.

6 IMAGING IN EMISSION LINES

Since optical images are also used to determine the radius of a nebula, the conversion factors for these images will be investigated as well. For this the same model was used as discussed in the previous section. The emissivity was assumed to be the volume emissivity of the following emission lines: Hα, Hβ, [N II] $\lambda6548$, $\lambda6584$ and [O III] $\lambda5007$. The contribution of continuum emission in the images was neglected. When solving the radiative transport equations, continuum optical depth effects were included, but not line optical depth effects. Next, the surface brightness profiles were computed for images taken in pure Hα light, in Hα+[N II] $\lambda\lambda6548$, 6584, in Hβ and in [O III] $\lambda5007$. The results are shown in the upper panel of Fig. 6. Finally, the conversion factors were computed for these profiles. The parameters for the fits are given in Table 3, the curves are shown in the lower panel of Fig. 6.
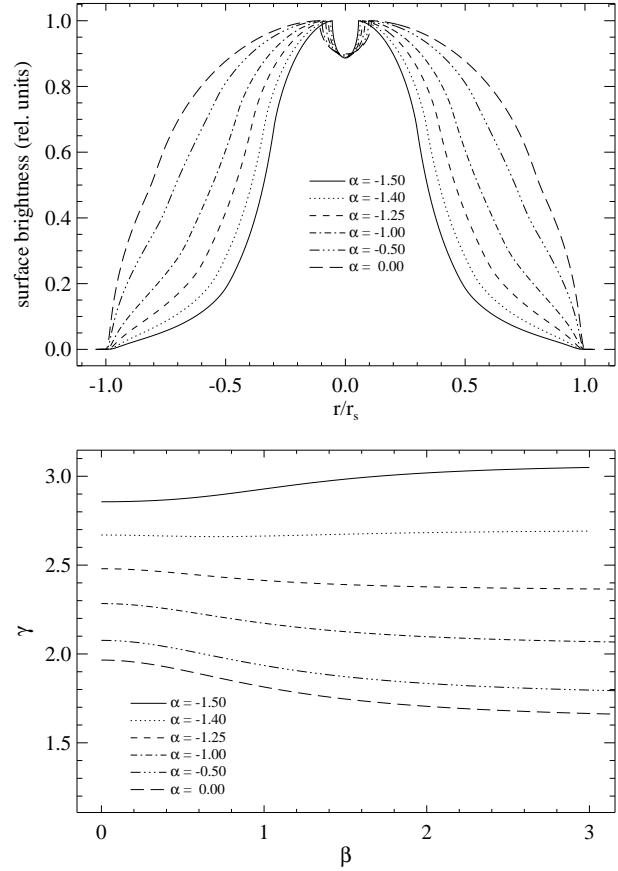
The first thing that can be noticed is that the surface brightness profiles in the various emission lines look completely different and that they also differ from the radio sur-

Figure 6. The intrinsic surface brightness profiles (upper panel) and the conversion factors (lower panel) in various emission lines. The maximum surface brightness has been normalized to unity. The conversion factors for the 2 cm radio image are also shown for reference.

Figure 7. The intrinsic surface brightness profiles (upper panel) and the conversion factors (lower panel) for different density distributions. The maximum surface brightness has been normalized to unity.

face brightness profiles shown in Fig. 5. Also the positions for the peak surface brightness are completely different. This implies that even in well-resolved images, the measured diameter can be different depending on which line is used. This is a well known effect caused by ionization stratification. Given this, it can already be expected that the conversion factors should be different for the various images as well, which is indeed confirmed. The conversion factors for images in pure Hα and Hβ light are nearly identical, which can be expected from the fact that the relative level populations depend only mildly on electron temperature and density. However, this situation completely changes when the [N II] lines are included in the passband of the Hα filter (as is usually the case). This has a considerable effect on the conversion factor. Also the conversion factors for the [O III] image are quite different from the Hβ case, but, by chance, nearly coincide with the values for the Hα+[N II] image. It can be seen that all conversion factors for the optical images are considerably smaller than the values for the (optically thin) 2 cm radio image.

From this the conclusion can be drawn that angular diameters measured in different images (including radio observations) can *not* be compared directly, even when they are well-resolved. In general the conversion factors for the

Table 4. The parameters for calculating the conversion factors for various density profiles. The conversion factors for gaussian deconvolution can be calculated using Eq. (5), the conversion factors for second moment deconvolution can be calculated using Eq. (7). The diameter is given in arbitrary units.

α	Θ_d	a_1	a_2	a_3
0.00	1.137	0.3428	0.7853	1.6222
-0.50	1.261	0.3188	0.7911	1.7573
-1.00	1.504	0.2418	0.8397	2.0415
-1.25	1.747	0.1253	1.1091	2.3545
-1.40	1.994	-0.078	0.078	2.740
-1.50	2.250	-0.252	0.476	3.103

various images will be different, depending on the intrinsic surface brightness profile and the beam size of the observation. For the cases that have been studied above, differences exceeding 30 % are possible.

7   NON-CONSTANT DENSITY GEOMETRIES

The nebular model that has been discussed so far assumes a constant hydrogen density within the ionized region. This automatically leads to a well-defined boundary of the neb-

ula. To investigate how the conversion factors behave for nebulae with soft boundaries, the density law was changed in the following way. For the inner parts of the nebula [lg(r/cm) < 16.6] the density law remained unchanged (i.e. constant), but for the outer parts an r^α law was assumed. This roughly models a nebula where the inner parts have undergone hydrodynamic interactions with the fast post-AGB wind, but where the outer parts are not yet disturbed. Values of α were used ranging from 0.0 down to -1.5. All the other parameters of the model were kept unaltered. For all models a radio image was calculated at a wavelength of 2 cm. The surface brightness profiles and conversion factors are shown in Fig. 7. In Table 4 the parameters for the fits to the conversion factors together with the true angular diameters of the nebulae can be found.

The first thing that can be noticed is that the conversion factor becomes increasingly larger as α becomes more negative. This can be easily understood when the nature of the changes to the density profile are viewed. Since a large part of the constant density regime within the ionized region remains unaltered when α is changed, also the high surface brightness core of the nebula remains more or less unaltered. Since the FWHM is mainly determined by the core region, the deconvolved FWHM will not change much as a function of α. However, the Strömgren radius is very sensitive to α, as can be seen in Table 4. This implies that the conversion factor must also be a sensitive function of α. If the Strömgren radius is chosen as a physically meaningful radius, this makes it almost impossible to measure this radius from low resolution observations if density distributions similar to the ones discussed here are suspected. It is the authors opinion that in such a case the only meaningful thing to do is to publish the deconvolved FWHM and the beam size and not to make any attempt to calculate the Strömgren radius.

8   A NEW ALGORITHM TO DETERMINE THE INTRINSIC FWHM

In Paper I it has been shown that the deconvolved FWHM obtained from second moment deconvolution is independent of the beam size, and therefore equal to the (second moment) FWHM of the intrinsic profile. Hence this method has the advantage that the FWHM of the unconvolved profile can be obtained directly from the observations without making any assumptions about the shape of the profile. Both from Paper I and this paper it has become clear that gaussian deconvolution does *not* have this property and assumptions about the intrinsic profile are always necessary. From the previous section it is also clear that such assumptions are not always warranted. This situation is not very satisfactory, and therefore a new algorithm will be presented here which will remedy this problem. This algorithm will yield the (gaussian fit) FWHM of the intrinsic profile, given the observed profile and the FWHM of the beam, without making any assumptions about the intrinsic profile. To use this method one has to determine the radial moments $c_{2n}{}'$ of the observed (i.e., convolved) profile and convert them to the radial moments of the intrinsic (i.e., unconvolved) profile c_{2n}. The radial moments $c_{2n}{}'$ are related to c_{2n} by Eq. (9).

$$c_{2n}{}' = \sum_{k=0}^{n} \frac{n!^2}{(n-k)!\,k!^2}\,\frac{c_{2k}}{p^{n-k}}; \quad p \equiv \frac{4\ln 2}{\Phi_{\rm b}^2} \quad \Rightarrow \qquad (9)$$

$$c_0{}' = c_0, \quad c_2{}' = c_2 + \frac{c_0}{p}, \quad c_4{}' = c_4 + \frac{4c_2}{p} + \frac{2c_0}{p^2}, \quad \cdots$$

This relation can easily be inverted

$$c_0 = c_0{}', \quad c_2 = c_2{}' - \frac{c_0{}'}{p}, \quad c_4 = c_4{}' - \frac{4c_2{}'}{p} + \frac{2c_0{}'}{p^2}, \quad \cdots$$

These relations constitute the actual deconvolution. In order to obtain the FWHM of the deconvolved profile (which we will call the intrinsic FWHM), the values of c_{2n} resulting from this calculation have to be substituted in Eq. (8). A derivation of this algorithm is presented in Sections 4 and 5 of Paper I. This method uses the fact that information about the intrinsic profile is implicitly contained in the radial moments of the convolved profile, and will therefore be called implicit deconvolution.

In the remainder of the section this method will be tested on artificial data. To this end the three simple geometries that where already discussed in Section 4 will be used. In order to simulate realistic observing conditions, these surface brightness distributions were convolved with a gaussian beam of prescribed width and observational noise was added using a Poisson noise generator. For this the photon count of the peak surface brightness was prescribed. Additionally a read-out noise of 6 counts was assumed. The pixel scale of the CCD was chosen such that in each case the FWHM of the beam corresponded to approximately 5 pixels. The results of the tests are shown in Table 5. Before the results of the implicit deconvolution method will be discussed, first two remarks will be made concerning the alternative method to measure the FWHM (given by Eq. (8)).

In Paper I it was shown that this method yields identical results to a gaussian fit algorithm. This is true when the profile is perfectly sampled. However, in real data the profile is only partially sampled and this may lead to small discrepancies between the two methods on the order of the measurement uncertainty in the FWHM.

A second concern is that, due to noise, negative values for pixels can occur in the low surface brightness areas. The theory presented in Paper I is strictly speaking not valid for such profiles. In practice however, this was found not to give any problems. All measurements of the convolved FWHM (Φ) presented in Table 5 converged, even in the poorest signal-to-noise conditions.

The results in Table 5 show that the implicit deconvolution method gives stable results in realistic conditions, provided the beam size is less than roughly 2/3 of the observed FWHM. The accuracy of the resulting intrinsic FWHM can be judged by comparing it to the results in Table 2. By looking at the high signal-to-noise results, one can see that small discrepancies can occur. These can be attributed to the fact the observed profile was only sampled with a very small number of pixels, as was discussed above. It is interesting to note that the implicit deconvolution method is not hampered by low signal-to-noise conditions, in the sense that the maximum beam size for which the method still works is hardly affected by low signal-to-noise conditions. It is therefore concluded that the implicit deconvolution method works well in realistic conditions, even when the signal-to-noise is low, provided that the beam size is less

Table 5. The results from the implicit deconvolution method for a disk, sphere and shell geometry as defined in Section 3. The number following the name of the geometry indicates the photon count at the maximum surface brightness. Φ_b indicates the FWHM of the beam, Φ the FWHM of the convolved profile and Φ_{in} the intrinsic FWHM. In each case the measurements were repeated 24 times using a different seed for the random generator; the quoted FWHM is the average of all cases where the method converged, σ indicates the standard deviation (68 % confidence interval) of an individual measurement. Cases where the implicit deconvolution method converged less than 12 times are omitted from the table. In all cases the beam size is assumed to be measured with high accuracy.

	disk − 500				disk − 5000				disk − 50000			
Φ_b	Φ	σ	Φ_{in}	σ	Φ	σ	Φ_{in}	σ	Φ	σ	Φ_{in}	σ
0.25	1.493	0.006	1.486	0.006	1.4930	0.0014	1.4858	0.0014	1.4934	0.0005	1.4861	0.0006
0.35	1.501	0.011	1.486	0.011	1.5021	0.0025	1.4866	0.0026	1.5021	0.0008	1.4867	0.0009
0.50	1.520	0.012	1.485	0.013	1.5200	0.0038	1.4856	0.0041	1.5211	0.0013	1.4868	0.0013
0.71	1.563	0.018	1.481	0.023	1.5672	0.0054	1.4871	0.0068	1.5686	0.0016	1.4887	0.0020
1.00	1.673	0.032	1.476	0.043	1.6808	0.0084	1.4902	0.0132	1.6822	0.0026	1.4921	0.0039
1.41	1.917	0.045			1.9261	0.0116			1.9276	0.0035		

	sphere − 500				sphere − 5000				sphere − 50000			
Φ_b	Φ	σ	Φ_{in}	σ	Φ	σ	Φ_{in}	σ	Φ	σ	Φ_{in}	σ
0.25	1.296	0.008	1.284	0.008	1.2946	0.0019	1.2832	0.0019	1.2949	0.0007	1.2834	0.0011
0.35	1.313	0.012	1.288	0.013	1.3132	0.0034	1.2885	0.0037	1.3137	0.0011	1.2890	0.0012
0.50	1.335	0.012	1.282	0.014	1.3365	0.0042	1.2842	0.0048	1.3379	0.0013	1.2857	0.0015
0.71	1.395	0.022	1.277	0.031	1.4013	0.0058	1.2862	0.0085	1.4025	0.0018	1.2875	0.0026
1.00	1.536	0.033			1.5433	0.0087	1.2956	0.0169	1.5447	0.0027	1.2926	0.0054
1.41	1.815	0.043			1.8240	0.0114			1.8254	0.0035		

	shell 0.8 − 500				shell 0.8 − 5000				shell 0.8 − 50000			
Φ_b	Φ	σ	Φ_{in}	σ	Φ	σ	Φ_{in}	σ	Φ	σ	Φ_{in}	σ
0.25	1.637	0.007	1.633	0.007	1.6366	0.0014	1.6326	0.0014	1.6370	0.0004	1.6330	0.0004
0.35	1.641	0.010	1.632	0.010	1.6415	0.0023	1.6326	0.0024	1.6416	0.0007	1.6328	0.0008
0.50	1.652	0.012	1.631	0.012	1.6522	0.0037	1.6311	0.0038	1.6532	0.0012	1.6322	0.0012
0.71	1.682	0.014	1.628	0.016	1.6845	0.0045	1.6313	0.0052	1.6858	0.0014	1.6327	0.0016
1.00	1.766	0.029	1.625	0.037	1.7747	0.0077	1.6336	0.0095	1.7760	0.0023	1.6347	0.0033
1.41	1.981	0.044			1.9917	0.0114			1.9932	0.0035		

than roughly 2/3 of the observed FWHM and the beam profile can be approximated by a gaussian. It can be a good alternative for gaussian deconvolution of partially resolved sources, since it requires no assumptions on the intrinsic surface brightness distribution. However, in order to convert the intrinsic FWHM of the source into the Strömgren diameter, knowledge about the intrinsic surface brightness distribution is still needed. A FORTRAN program implementing the algorithm discussed in this section is available from `ftp://gradj.pa.uky.edu/pub/peter/genfit.f`.

9 CONCLUSIONS

In this work conversion factors have been determined to convert the deconvolved FWHM of a partially resolved nebula to its true diameter. It was already found by Mezger & Henderson (1967) that this conversion factor depends on the (assumed) intrinsic surface brightness profile of the nebula. In a subsequent study by Panagia & Walmsley (1978) it was found that the conversion factor also depends on the beam size of the observation when gaussian deconvolution is used. This paper expands on previous work in that an alternative method for deconvolving the FWHM, second moment deconvolution, is studied for the first time. Also the influence of the intrinsic surface brightness profile on the conversion factor is studied in more detail. The following recommendations and conclusions were reached. Unless explicitly noted otherwise, they are valid both for gaussian and second moment deconvolution and also for observations at arbitrary wavelengths.

(i) When making a gaussian fit to a surface brightness profile, it is recommended to use a diameter for the fitting region which is at least 3 times the FWHM diameter of the fit in all cases. A larger fitting region should be used if extended faint emission is present. In order to obtain an accurate value for the FWHM of an observed source, it is essential that the global background in the image is subtracted first so that it can assumed to be zero in the fitting procedure. Trying to determine the FWHM and the background simultaneously in the fitting procedure is found to give very poor results.

(ii) The deconvolved FWHM derived using gaussian fits is in general not equal to the deconvolved FWHM derived using second moments. Hence the conversion factors will also be different in both cases. For second moment deconvolution, the conversion factor is *independent* of the beam size. Its value is in all cases equal to the conversion factor for the gaussian deconvolution method in the limit for infinitely large beams. The conversion factor for second moment deconvolution does depend on the assumed surface brightness profile.

(iii) The conversion factor is very sensitive to the adopted intrinsic surface brightness profile. Differences up to 40 % can be found for constant emissivity shells with different inner radii. Hence, great care should be taken when making a choice for the intrinsic surface brightness distribution.

(iv) Because of this, observers are urged to publish, besides the Strömgren diameter of the nebula, the deconvolved FWHM, the method used (i.e. gaussian or second moment deconvolution) *and* the beam size.

(v) The conversion factor is very sensitive to optical depth effects, so care should be taken when comparing observations made at different wavelengths. This is especially the case for radio observations. Differences of several tens of percent are possible.

(vi) For optical observations the conversion factor depends on which emission line is chosen. This is partly due to ionization stratification and this results in the fact that even

well-resolved images in different emission lines can yield different diameters. It is also caused by the fact that the intrinsic surface brightness profile is different in different emission lines. Again differences of several tens of percent are possible. Hence care should be taken when comparing optical and radio measurements.

(vii) Nebulae which have a power law drop-off in their density distribution usually do not have a well-defined outer edge and the Strömgren radius will be situated in the faint surface brightness regions of the nebula. For such nebulae the conversion factor can become very large and is very sensitive to the assumed intrinsic surface brightness distribution of the nebula. Since this distribution can in general not be assessed accurately, it is not meaningful to apply a conversion factor and only the deconvolved FWHM and the beam size should be published.

Finally, in this paper a new algorithm has been presented which allows the determination of the intrinsic FWHM of the source, using only the observed surface brightness distribution and the FWHM of the beam. More in particular, no assumptions with regard to the intrinsic surface brightness distribution are needed. This makes the method a good alternative for gaussian deconvolution. Tests show that the implicit deconvolution method works well in realistic conditions, even when the signal-to-noise is low, provided that the beam size is less than roughly 2/3 of the observed FWHM and the beam profile can be approximated by a gaussian.

REFERENCES

Bedding T.R., Zijlstra A.A., 1994, A&A, 283, 955 (BZ)
Beintema D.A., van Hoof P.A.M., Lahuis F., Pottasch S.R., Waters L.B.F.M., de Graauw T., Boxhoorn D.R., Feuchtgruber H., Morris P.W., 1996, A&A, 315, L253
Falomo R., 1996, ESO Messenger, 86, 37
Ferland G.J., 1993, University of Kentucky, Physics Department, Internal Report
King I.R., 1971, PASP, 83, 199
Mezger P.G., Henderson A.P., 1967, ApJ 147, 471 (MH)
Panagia N., Walmsley C.M., 1978, A&A 70, 411 (PW)
Pottasch S.R., 1984, Planetary Nebulae, Reidel, Dordrecht, p. 88
Schneider S.E., Buckley D., 1996, ApJ 459, 606 (SB)
van Hoof P.A.M., 1999, University of Kentucky, Dept. of Physics and Astronomy, Internal Report (Paper I, astro-ph/9906051)
Wellman G.F., Daly R.A., Wan L., 1997, ApJ 480, 79